

pLUTo: Enabling Massively Parallel Computation In DRAM via Lookup Tables

João Dinis Ferreira[§]

Gabriel Falcao[†]

Juan Gómez-Luna[§]

Mohammed Alser[§]

Lois Orosa[§]

Mohammad Sadrosadati[§]

Jeremie S. Kim[§]

Geraldo F. Oliveira[§]

Taha Shahroodi^{§‡}

Anant Nori^{*}

Onur Mutlu[§]

[§]ETH Zürich [†]Instituto de Telecomunicações, University of Coimbra [‡]TU Delft ^{*}Intel Corporation

Data movement between main memory and the processor is a key contributor to the execution time and energy consumption of memory-intensive applications. This data movement bottleneck can be alleviated using Processing-in-Memory (PiM). One category of PiM is Processing-using-Memory (PuM), in which computation takes place inside the memory array by exploiting intrinsic analog properties of the memory device. PuM yields high throughput and efficiency, but supports a limited range of operations. As a result, PuM architectures cannot efficiently perform some complex operations (e.g., multiplication, division, exponentiation) without sizeable increases in chip area and design complexity.

To overcome this limitation in DRAM-based PuM architectures, we introduce pLUTo (processing-using-memory with lookup table (LUT) operations), a DRAM-based PuM architecture that leverages the high area density of DRAM to enable the massively parallel storing and querying of lookup tables (LUTs). The use of LUTs enables pLUTo to efficiently execute complex operations in-memory via memory reads (i.e., LUT queries) instead of relying on complex extra logic or performing long sequences of DRAM commands. pLUTo outperforms the optimized CPU and GPU baselines in performance/energy efficiency by an average of 1960×/307× and 4.2×/4× across the evaluated workloads, and by 33×/8× and 110×/80× for the LeNet-5 quantized neural network. pLUTo outperforms a state-of-the-art PiM baseline by 50×/342× in performance/energy efficiency.

1. Introduction

Processing-in-Memory (PiM) is a promising paradigm that augments a system’s memory with compute capability [48, 50, 88, 89, 113] to alleviate the *data movement bottleneck* between the processing units and the memory units of computing systems [26, 32, 66, 80, 89, 93, 99, 116, 119, 122]. PiM architectures can be classified into one of two categories [50]: 1) **Processing-near-Memory (PnM)**, where computation takes place in processing elements located *near* the memory array [35, 62, 74, 79, 85, 100, 105], and 2) **Processing-using-Memory (PuM)**, where computation takes place *inside* the memory array by exploiting intrinsic analog properties of the memory device [33, 46, 54, 83, 106, 108].

In PnM architectures, data is transferred from the DRAM to nearby processors or specialized accelerators, which are either 1) part of the DRAM chip, but separate from the memory

array [35, 74], e.g., near the DRAM banks, or 2) integrated into the logic layer of 3D-stacked memories [62, 85]. PnM enables the design of flexible substrates that support a diverse range of operations. However, the design and fabrication of PnM architectures is subject to significant challenges that limit their performance and scalability. For example, in near-bank PnM architectures [35, 74], the limited number of metal layers in DRAM [101, 121] impedes the fabrication of fast logic transistors [35, 52] for the near-bank processors. In 3D-stacked memories, the limited area and thermal budget of the logic layer impose additional constraints. All these design and fabrication issues lead to wimpy PnM cores, which cannot exploit the entire DRAM bandwidth [37, 52, 92].

In contrast, PuM architectures enable computation *within* the memory array. The key benefit of PuM architectures is that *data does not leave the memory unit during computation*. As a result, PuM architectures can provide high compute throughput by performing operations in a bulk parallel manner, often at the granularity of memory rows. Prior PuM works propose mechanisms for the execution of bitwise operations (e.g., AND/OR/XOR) [46, 106, 108] and arithmetic operations [33, 34, 83, 114]. However, these proposals result in high latency and energy consumption for the execution of some complex operations (e.g., multiplication, division) [54], while other operations (e.g., exponentiation, binarization) are not supported.

One approach to increase the operation support and/or their efficiency in PuM architectures is to perform computation using lookup tables (LUTs) [34, 47]. Under *LUT-based computing*, the results of complex functions are precomputed or memoized and stored in a LUT. A *LUT query* is a *memory read operation* that returns the result of a function $f(x)$ for an input value x . Several prior PuM architecture proposals [34, 47, 114] exploit LUT-based computing to improve the performance of specific complex operations (e.g., multiplication [34]). However, none of these proposals provides support for the general-purpose execution of LUT-based complex operations.

Our goal in this work is to *extend the functionality of DRAM-based PuM to provide support for complex operations via the bulk querying of LUTs*. **To this end**, we propose pLUTo: *processing-using-memory with lookup table (LUT) operations*, a DRAM-based PuM architecture that leverages LUT-based computing to perform complex operations beyond the scope of

prior PuM proposals. pLUTo introduces a novel LUT-querying mechanism, the *pLUTo LUT Query*, which enables the simultaneous querying of multiple LUTs stored in a single memory array. Each LUT may contain up to as many entries as there are rows in each memory subarray (for DDR4, about 512 rows [70]). The design of pLUTo requires the following two reasonable modifications to DRAM hardware: 1) **row sweeping logic**, which enables the *sweeping* of memory rows, i.e., the successive activation of consecutive memory rows in a memory array; 2) **match logic**, which identifies *matches* between the *elements* in the input row and the *index* of the currently active row in the subarray which holds the LUTs. We describe three pLUTo designs: pLUTo-GSA, pLUTo-BSA, and pLUTo-GMC. Each of these designs achieves a different trade-off between area overhead and performance/energy efficiency. To enable a seamless integration of pLUTo with the system, we describe the stack of changes that enables a programmer to offload their applications to pLUTo: this encompasses 1) the development of source code which includes pLUTo ISA instructions, 2) a compiler which analyzes the application’s data dependency graph to determine the optimal intra- and inter-row data allocation mapping, and 3) a pLUTo controller and runtime library that monitor the allocation of pLUTo data structures and oversee the execution of pLUTo operations throughout the application’s runtime.

We evaluate pLUTo for a diverse range of operations, including bitwise (e.g., AND/OR/XOR), arithmetic (e.g., 4-bit addition and multiplication), and nonlinear functions (e.g., cryptographic substitution tables, image binarization, and LUT-based image color grading). We compare pLUTo to state-of-the-art processor-centric architectures (CPU [63], GPU [91], FPGA [125]) and PiM architectures (PnM [62], PuM [54, 83, 108]) across four arithmetic operations (4- and 8-bit addition, 8- and 16-bit fixed-point multiplication), seven workloads (e.g., 8-, 16-, and 32-bit CRC, Image Binarization, Image Color Grading), and one quantized neural network case study. Our evaluations show that pLUTo consistently outperforms these baselines, especially when normalizing to area overhead. We make the following **key contributions**:

- We introduce pLUTo, a DRAM-based PuM architecture that enables support for general-purpose LUT-based general-purpose/complex operations.
- We propose three different pLUTo designs with different trade-offs in area overhead, energy efficiency, and performance.
- We describe the end-to-end system integration of pLUTo, which encompasses a set of ISA extensions, the specification for the compilation procedure of pLUTo source code, and dedicated hardware structures that augment DRAM with the required bookkeeping abilities.
- We evaluate pLUTo using arithmetic, bitwise logic, cryptographic, image processing, and neural network workloads and compare it to CPU [63], GPU [91], FPGA [125], and recent PiM [54, 62, 83, 108] architectures.

2. Background

This section describes the hierarchical organization of DRAM and provides an overview of relevant prior work.

2.1. DRAM Background

A DRAM chip contains multiple memory *banks* (8 for DDR3, 16 for DDR4), and I/O circuitry. As shown in Figure 1, each bank is further divided into *subarrays*, which are two-dimensional arrays of memory cells. The DRAM subarrays in a bank share peripheral circuitry (e.g., row decoders). Each *cell* contains one capacitor and one access transistor. The capacitor encodes a single bit as stored electrical charge. The memory cell transistor connects the capacitor to the *bitline* wire. Each bitline is shared by all memory cells in a column, and connects to a *sense amplifier*. The set of sense amplifiers in a subarray makes up the *local row buffer*.

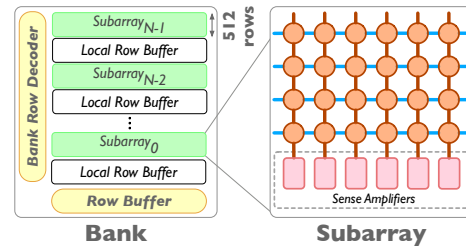


Figure 1: The internal organization of DRAM banks.

Reading and writing data in DRAM occurs over three phases: 1) Activation, 2) Reading/Writing, 3) Precharging. During Activation, the wordline of the accessed row is driven high. This turns on the row’s *access transistors* and creates a path for charge sharing between each memory cell and its bitline. This process induces a voltage fluctuation ($\pm\delta$) in the bitline, which is originally set at $V_{DD}/2$. If the cell is charged, the bitline voltage becomes $V_{DD}/2 + \delta$. Otherwise, it becomes $V_{DD}/2 - \delta$. To read the value of the cell, the sense amplifiers in the local row buffer amplify the fluctuation ($\pm\delta$) recorded by the bitline during Activation. Simultaneously, the original charge level is restored to the memory cell’s capacitor. After reading, data is sent to the CPU through the I/O circuitry and the memory bus. During Precharging, the access transistors are turned off, and all bitlines are restored to $V_{DD}/2$.

2.2. DRAM Extensions

pLUTo optimizes key operations by incorporating the following previous proposals for enhanced DRAM architectures.

Inter-Subarray Data Copy. The *LISA-RBM* (Row Buffer Movement) operation [30] copies the contents of one row buffer to another row buffer in a different subarray, without relying on the external memory channel. This is achieved by linking neighboring subarrays with isolation transistors.

Subarray-Level Parallelism. *MASA* [70] is a mechanism that enables subarray-level parallelism by overlapping the latency of memory accesses directed to different subarrays.

Bitwise Operations. *Ambit* [108] introduces support for bulk bitwise logic operations between rows in a DRAM subarray.

Shifting. DRISA [83] introduces support for intra-row shifting in DRAM. Using this mechanism, the contents of a memory row may be shifted by 1 or 8 bits at a time, with a cost of *one* Activate-Activate-Precharge (AAP) command sequence.

3. Motivation

Our goal in this work is to introduce support for the in-memory execution of general-purpose operations. In particular, pLUTo is motivated by the following two key observations. First, state-of-the-art PuM architectures [34, 83, 108] provide very high throughput and energy efficiency by mitigating data movement, but only support a limited range of operations. For example, state-of-the-art in-situ DRAM-based specialized accelerators only support the execution of basic operations (e.g., addition, bitwise logic) [83, 108] or employ long sequences of DRAM commands for more complex operations (e.g., multiplication, division) [54]. Second, LUTs can replace complex computations with cheaper lookup queries (i.e., memory reads). pLUTo improves prior PuM works by leveraging their best features (i.e., high parallelism, reduced data movement) and addressing their main drawbacks (i.e., reduced range of supported operations and low performance/lack of support for complex operations), and achieves this via the introduction of the pLUTo LUT Query operation, which enables the simultaneous querying of all the values in a given input memory row in bulk.

4. An Overview of pLUTo

The key contribution of pLUTo is the *pLUTo LUT Query*, a mechanism that enables the simultaneous execution of a large number of table lookups *inside* the memory array. To understand this operation, we first discuss the data layout of the involved operands in memory, as shown in Figure 2. Figure 2 (a) shows an overview of the DRAM structures required to support pLUTo’s operation. Three subarrays are involved: 1) the *source subarray*, which stores input data for the pLUTo LUT Query, 2) the *pLUTo-enabled subarray*, which stores the LUTs to be queried, and 3) the *destination subarray*, to which the output data will be copied. LUT data is stored in the pLUTo-enabled subarray as depicted in Figure 2 (b), i.e., so that *consecutive LUT entries* are stored in *consecutive memory rows* in the pLUTo-enabled subarray. For each LUT entry, all the bits are stored *horizontally* (i.e., all in the same memory row).

The pLUTo LUT Query. The pLUTo LUT Query enables all the elements stored in a *source row* to query a LUT. We illustrate the pLUTo LUT Query using a small example, which employs a small LUT to store four prime numbers {2, 3, 5, 7} at indices {0, 1, 2, 3}, as shown in Figure 3 (a). Four copies of this LUT are stored in a pLUTo-enabled subarray, as shown in Figure 3 (b): each row i contains repeated copies of the element corresponding to the entry at the i -th index of the LUT. pLUTo performs a pLUTo LUT Query with an example input vector with values {1, 0, 1, 3}, for which the output will

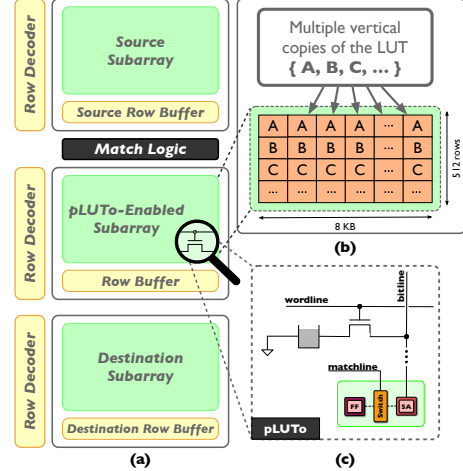


Figure 2: (a) Main components of pLUTo. (b) LUT layout inside a pLUTo-enabled subarray. (c) Design of the pLUTo cell and sense amplifier.

be the prime number sequence {3, 2, 3, 7}, in three steps. First, the memory controller loads the input values from the source subarray (not shown) into the source row buffer, as shown in Figure 3 (b). Second, the memory controller issues a *row sweep* operation (see Section 5.1.1) to quickly activate all rows that hold LUT entries in sequence; after each activation, the match logic checks for matches between the elements of the source row buffer (i.e., the input vector of LUT indices) and the index of the currently activated row in the pLUTo-enabled subarray. If there is a match (see ① in Figure 3 (c)), the contents of the activated row *at the matching locations* are copied to the destination row buffer (see ② in Figure 3 (c)). Third, the results of the pLUTo LUT Query are copied to the destination row using a LISA-RBM command (see ③ in Figure 3 (c)), as described in Section 2.2.

5. pLUTo: A DRAM-based PuM Architecture

We introduce the architecture of pLUTo, which enables the execution of basic pLUTo LUT Queries, and how we combine it with available PuM-based operations [30, 70, 83, 108].

5.1. pLUTo Architecture

To enhance a DRAM subarray with pLUTo operations, we 1) change the row decoders and row buffer, and 2) build a *match logic* unit that compares the values of each entry in the source row with the value of the currently activated row and identifies matches.

5.1.1. pLUTo-Enabled Row Decoder. To enhance the DRAM row decoder, we enable a new functionality: *row sweep*. Row sweep extends the self-refresh operation which already exists in commodity DRAM [75] to quickly activate many consecutive rows in sequence. The latency of the row sweep operation is equal to $(t_{RAS} + t_{RP}) \times N$, where t_{RAS} is the time that must elapse between an activate and a precharge command, t_{RP} is the latency that must elapse between a precharge command and the next activate command, and N is the total

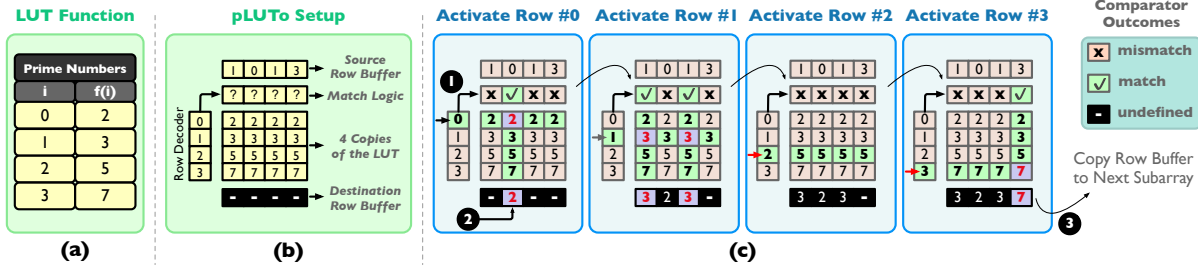


Figure 3: A pLUTo LUT Query: (a) a LUT containing the first four prime numbers, (b) the pLUTo-enabled subarray, and (c) steps of the pLUTo LUT Query. This pLUTo LUT Query returns the i -th prime number for each element in the input row.

number of rows swept. This operation enables the quick matching and querying of data of across many rows.

5.1.2. pLUTo-Enabled Row Buffer. In DRAM, each sense amplifier in the row buffer can only one value, following the activation of a memory row; this is not sufficient for the execution of the row sweeping operation, given the necessity to store intermediate results corresponding to index matches as they become available, following each row activation. To enhance DRAM row buffer with support for this, we connect one additional flip-flop (FF) to every sense amplifier in the row buffer via a switch (shown in Figure 2 (c)). The set of FFs constitutes a *FF buffer*. If a switch is enabled by the *matchline* signal, data in the sense amplifier is copied to the corresponding FF. As we can drive each matchline signal independently, data in the row buffer can be partially written to the FF buffer. This capability enables more complex data management operations such as gather-scatter, which we use to enable our new LUT-based operations.

5.1.3. pLUTo-Enabled Match Logic. As shown in Figure 2 (a), we implement match logic between subarrays that consist of an array of two-input comparators: 1) the index of the currently activated row in a pLUTo-enabled subarray and 2) an element in another *source* subarray. Each comparator outputs N matchline signals, where N is the bit width of each LUT entry. Each matchline connects to the switch belonging to the corresponding FF in the pLUTo-enabled row buffer, as shown in Figure 2 (c). If the two inputs of the comparator match, each of the N output matchlines from the comparator are driven high. Otherwise, the matchlines are driven low.

5.2. Subarray-Level Parallelism

pLUTo’s performance can be further improved by leveraging parallelism *across* subarrays, as demonstrated in MASA [70] (see Section 2.2). The degree of parallelism that can be achieved is limited by the JEDEC DRAM Standard [64, 65], which specifies a limit for the rate of issuance of activate commands. This limit is dictated by the tFAW timing parameter, which indicates the time window during which *at most four* activate commands can be issued, per DRAM rank. This constraint prevents the deterioration of the DRAM reference voltage. DRAM manufacturers have been able to reduce the value of tFAW in DDR3 chips in recent years [87]. This may

be possible through the use of more powerful charge pumps.

5.3. Alternative pLUTo Architectures

To offer more flexibility to the system architect, we provide two additional variants to the pLUTo architecture with different trade-offs in throughput, area efficiency, and energy efficiency: 1) pLUTo-GSA (Gated Sense Amplifier) and 2) pLUTo-GMC (Gated Memory Cell). We refer to the design presented in Section 5.1 as pLUTo-BSA (Buffered Sense Amplifier). Table 1 qualitatively tabulates the trade-offs of each design. Each design can be used in largely the same way as pLUTo-BSA. We explain the subtleties associated with each design next.

Table 1: Qualitative comparison of pLUTo designs.

	pLUTo-GSA	pLUTo-BSA	pLUTo-GMC
Area Efficiency	High	Medium	Low
Throughput	Low	Medium	High
Energy Efficiency	Low	Medium	High
Destructive Reads	Yes	No	No
Data Loading	After every use	Once	Once

5.3.1. pLUTo-GSA: Gated Sense Amplifier. pLUTo-GSA provides superior area efficiency over pLUTo-BSA, at the expense of reduced throughput and energy efficiency. pLUTo-GSA differs from pLUTo-BSA in its row buffer design and implementation of the row sweep operation.

pLUTo-GSA Row Buffer. Each sense amplifier in the pLUTo-GSA’s row buffer includes a switch that is controlled by the matchline signal and connects the sense amplifier to the bitline (Figure 4 (a)). When the switch is enabled, the sense amplifier can sense the value on the bitline. Since pLUTo-GSA does not use an FF buffer to aggregate data, this design has a smaller area overhead than pLUTo-BSA. However, activating cells connected to bitlines that are not attached to their respective sense amplifier (i.e., the matchline is driven low by the match logic) destroys their contents. Activations performed during the *row sweep* operation are thus potentially destructive, and hence LUTs must be loaded into the pLUTo-enabled subarrays before *every* pLUTo LUT Query.

Row Sweep Operation. Since row activations are destructive in pLUTo-GSA, the row sweep operation does *not* require issuing a precharge command following each activation. Instead, it is possible to issue a single precharge command at the end of the row sweep operation. The total time required to perform a row sweep in pLUTo-GSA is therefore

equal to $t_{RC} \times N + t_{RP}$, where t_{RC} is the minimum enforced time between two consecutive activate commands, t_{RP} is the precharge time, and N is the total number of rows swept. This is about half the time required for a row sweep operation compared to pLUTo-BSA.

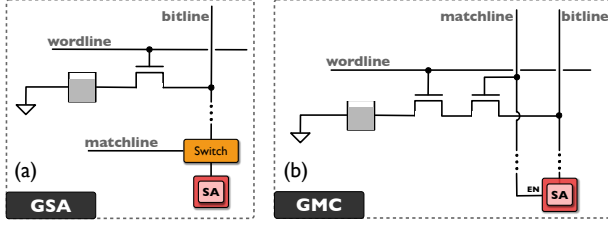


Figure 4: pLUTo-GSA (a) and pLUTo-GMC (b) designs.

5.3.2. pLUTo-GMC: Gated Memory Cell. pLUTo-GMC provides superior throughput and energy efficiency over pLUTo-BSA, at higher area overhead. pLUTo-GMC differs from the pLUTo-BSA in its DRAM cell design, row buffer design, and implementation of the row sweep operation.

pLUTo-GMC DRAM Cell. pLUTo-GMC implements 2T1C memory cells, instead of the conventional 1T1C DRAM cell design (that is also used in both pLUTo-GMC and pLUTo-GSA). The additional transistor in each 2T1C memory cell is controlled by the matchline, as shown in Figure 4 (b). This enables fine-grained control of which cells in an activated row share charge with its respective bitline. This significantly contributes to minimizing the energy consumption of this design, but also requires a higher area overhead.

pLUTo-GMC Row Buffer. pLUTo-GMC places an additional switch between the sense amplifier and its enable signal, which is enabled by the matchline signal (shared by cells attached to the same bitline). This switch ensures that the sense amplifier does not drive a value on the bitline if the cell is not also attached to the bitline. This enables pLUTo-GMC to both perform back-to-back activations without a precharge and save on energy costs for enabling the sense amplifier.

Row Sweep Operation in pLUTo-GMC. Two key features of our pLUTo-GMC design enable it to perform the row sweep operation almost twice as fast as pLUTo-BSA, by using back to back activations without precharging. First, a sense amplifier is only enabled when there is a match in the corresponding match logic. This means that activations *only* disturb bitlines whose associated matchline signals are driven high and the remaining bitlines are *maintained* at the nominal bitline voltage level (in the precharged state). Second, since a LUT query only has one match in a LUT, the sense amplifier is only enabled for a single row activation during an entire pLUTo LUT Query. Therefore, we can guarantee that back to back activations will *not* open the gating transistors of any two cells sharing the same bitline, and thus will not destroy the data in the cell. As in pLUTo-GSA, the total time required to perform a row sweep in pLUTo-GMC is equal to $t_{RC} \times N + t_{RP}$. In addition, due to the presence of gating transistors, pLUTo-GMC does not destroy the data in the LUTs; this translates into considerable

performance gains, as there is no need to repeatedly load LUT data to the subarray.

5.4. Limitations of the pLUTo Subarray Design

For a single-subarray pLUTo LUT Query, the number of LUT entries can be increased up to the number of rows in the subarray. To query LUTs with a greater number of entries, it is possible to partition a pLUTo LUT Query across subarrays. Note that partitioning the query does not increase latency (since pLUTo operates on multiple subarrays simultaneously), but does increase energy N -fold, for a pLUTo LUT Query distributed across N subarrays. We reserve the exploration of this possibility for future work.

6. System Integration

This section describes pLUTo’s system integration stack, which enables pLUTo to interoperate seamlessly with the host system.

6.1. Extending the ISA: the pluto_op

All pLUTo LUT Queries (defined in Section 4) executed in a pLUTo-enabled DRAM have a one-to-one correspondence with a `pluto_op` instruction, defined as follows:

pluto_op(src, dst, lut_subarr, lut_size, lut_bitw)
`src` and `dst` are the physical addresses of the source and destination rows, respectively. `lut_subarr` is the physical address of the pLUTo-enabled subarray where the LUT is stored. `lut_size` is the number of LUT entries, i.e., the number of rows to sweep; for example, a 4-bit-input LUT contains $2^4 = 16$ elements, and thus requires the sweeping of 16 rows. `lut_bitw` specifies the bit width of the LUT entries; this value must be given in addition to `lut_size`, for example, due to the possibility that the 2^N LUT entries are zero-padded, and therefore have wider bit widths than N . The `pluto_op` instruction always operates at the granularity of DRAM rows, such that operating on an S -byte input requires $\lceil \frac{S}{DRAM\ row\ size} \rceil$ `pluto_op` instructions.

6.2. pLUTo API Code

Figure 5 shows a simple example of the implementation of the following multiply-and-add operation between three vectors A (2-bit), B (2-bit), and C (4-bit): $A \odot B + C$. A reference implementation in the C programming language is shown in Figure 5 (a). To express this program using pLUTo instructions, the programmer leverages the pLUTo API to express memory row operations as shown in Figure 5 (b). For added programmer convenience, the pLUTo API supports pseudo-instructions (e.g., `pluto_add`, `pluto_mul`) which the compiler can automatically translate to pLUTo instructions (i.e., `pluto_op`, bit shifting, bitwise logic). The pLUTo API may be extended by the programmer with additional pseudo-instructions by specifying the desired mapping between inputs and outputs using a LUT. Unlike the reference implementation, the pLUTo API source code requires: 1) the allocation of memory for the

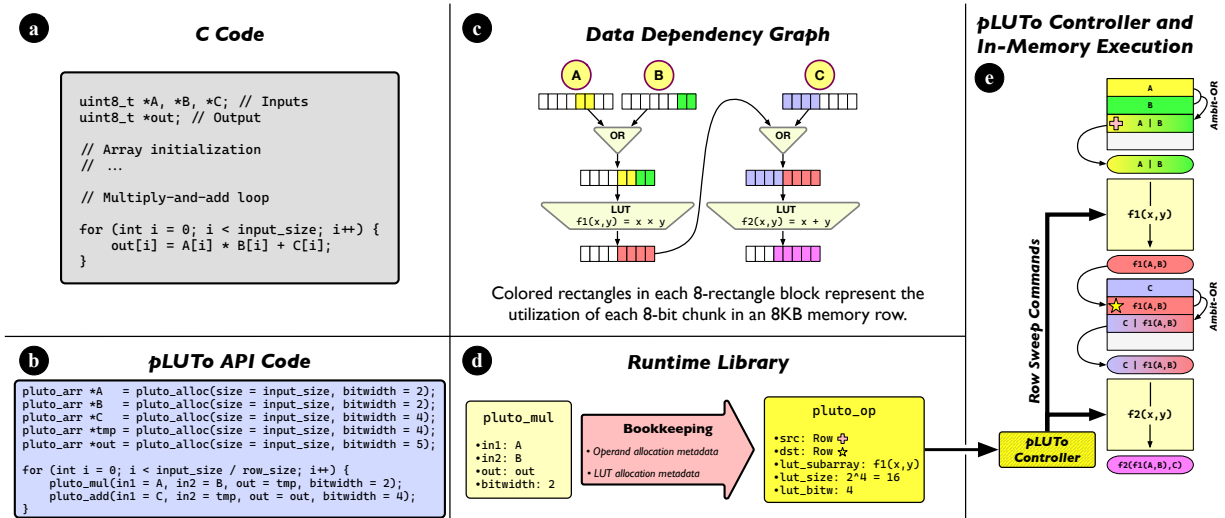


Figure 5: The role of pLUTo’s system integration stack, shown for the sample C code in (a). The subsequent steps consist of: (b) implementation using the pLUTo API; (c) analysis of the data dependency graph; (d) execution of the pLUTo runtime library; (e) operation of the pLUTo controller to enable in-memory execution. For brevity, (d) only shows the conversion of the multiplication operation to the corresponding pLUTo operation. The same procedure should be performed for the addition.

input (A, B, C), temporary (tmp), and output (out) arrays; 2) the execution of the desired vectorized operations using the provided abstractions (for the current example, element-wise multiplication and element-wise addition). This programming paradigm is analogous to CPU/GPU SIMD programming.

6.3. Data Dependency Graph: Operation Analysis

For added programmer ease-of-use, the compiler analyzes the data dependencies between pLUTo operands, and automatically determines 1) the DRAM row where they are stored, and 2) the DRAM intra-row data layout (i.e., the alignment of input elements in the input row, and the position of the significant bits in each input element). An example of one such optimization process is shown in Figure 5 (c), with the corresponding memory mapping depicted in Figure 5 (e). In the first stage of this example, 2-bit operands A and B are stored in the same subarray to perform a LUT-based element-wise multiplication. The 2 bits of information are stored in bits [3:2] for every byte of A; likewise, each element is stored in bits [1:0] for every byte of B. The intra-row data layout of these two operands allows them to be combined simply by performing an in-DRAM bitwise *Ambit-OR* [108] operation. In the second stage, the result of the first pLUTo LUT Query is copied to the subarray where operand C is stored. A similar procedure then takes place again, this time combining the result of the previous operation (whose 4-bit values are stored in bits [3:0] of every byte in the memory row) with operand C (whose 4-bit values are stored in bits [7:4] of every byte in the memory row). The output of this 4-bit element addition is a 5-bit value, as shown in the final result of Figure 5 (e). In general, three types of operations may be identified as a result of this analysis, which we now describe.

One-Shot Operations. Many common functions (e.g., arithmetic and nonlinear operations) can be directly expressed with LUTs. In such cases, it is possible to translate the API pseudo-instruction by 1) defining the function in question at compile time (e.g., the LUT to be used for color grading) 2) memoizing the results for all inputs, and 3) storing the ensuing results in a LUT. As a result, all inputs, outputs and LUTs can be allocated, instantiated, used, and deallocated automatically.

Two-Operand Functions. Another common type of operation involves the combination of two inputs. Consider the element-wise product of two vectors, as shown in the first pLUTo pseudo-instruction provided in Figure 5 (b). As in the one-shot scenario, it is possible to perform a one-time effort to memoize all results for any possible input, and to perform the associated LUT queries. In this case, however, there is a challenge concerning ideal data mapping: since the inputs to the LUT must be derived by combining two independent source arrays (stored in different memory rows), an additional step is required to combine them. This step can be trivially performed with a bitwise OR operation if, as shown in Figure 5 (c), the intra-byte alignment of the data in the two input vectors allows it. Therefore, one of the roles of the pLUTo compilation framework concerns the analysis of these data dependencies to determine the ideal mapping of data in advance. This is a well-understood problem in the domain of compilers (e.g., data dependency verification during register allocation [3]), and it is therefore straightforward to derive mappings that optimize the in-memory movement of data for real-world-sized sequences of pLUTo operations. In situations where it is not possible to immediately obtain the ideal mapping, an additional bit shifting step is required prior to the execution of the OR-based combination step. Since pLUTo supports bit shifting operations using the intra-lane shifting design pro-

posed in [83], this operation can be performed *in-situ* with low overhead.

Early Termination of the Row Sweep. During the course of a pLUTo LUT Query, if all the LUTs to be queried contain fewer entries than the number of rows in the pLUTo-enabled subarray where they are stored, it is possible to reduce the latency and energy cost of the pLUTo LUT Query operation by terminating the row sweep early. In effect, the number of rows to sweep is determined by *the bit width of each input element to be queried*. One convenient upshot of this is that pLUTo performs especially well for querying small LUTs. Each increase of 1 bit per input element causes the LUTs to contain twice as many entries, and therefore approximately doubles the latency and energy consumption of the pLUTo LUT Query.

6.4. Data Dependency Graph: Source Data

As shown in Figure 3 and discussed in Section 4, the pLUTo LUT Query requires that 1) the source row buffer, 2) the LUT subarray, and 3) the output row buffer be adjacent in memory. In addition, all input elements for a pLUTo LUT Query must reside in the same memory row.

For this reason, it is important to designate dedicated memory data structures to hold input/output data in a way that maximizes row utilization and, by extension, LUT utilization and operation efficiency. To this end, we define a custom memory allocation operation, the `pluto_alloc`, which allocates memory addresses while considering the above requirements. This operation reserves space in memory for an operand, and to do so receives 1) the size of this operand, in bytes, and 2) the bitwidth of each vector element. The allocation procedure then ensures that the vectors are allocated starting from the beginning of a memory row, and that they are interleaved in memory in a way that ensures the preservation of free space for the storage of the LUTs where the pLUTo LUT Query will be performed.

6.5. Data Dependency Graph: LUT Data

The LUTs associated with specific application segments that benefit from their use need to be loaded to the appropriate locations in DRAM. The ideal memory location for them is also determined as part of the data dependency graph analysis step. This is a four-step process: 1) identify the degree of parallelism supported by the memory; 2) coordinating the placement of LUT data such that it is in proximity to the subarrays that store source data; 3) compute the memory addresses for these LUTs, 4) copy the LUT contents to these memory locations upon application start-up, as soon as this data is available. The data to be stored in LUTs may become available in one of three ways:

Generation From Scratch. The first time a LUT is generated, all of its values must be computed from scratch. This procedure can be performed with lazy execution, for applications that require LUTs which cannot be pre-computed.

Loading From Memory. If a LUT already exists in memory, the most efficient way to reuse it is by copying it to the designated pLUTo-enabled subarray using LISA-RBM [30].

Loading From Secondary Storage. LUTs can be generated at compile-time and stored together with the application binary file. In this case, these LUTs can be loaded together with the application code from secondary storage into main memory at runtime, for example using a direct memory access (DMA) operation. We evaluate this process in Section 8.5.

6.6. Runtime Library

As shown in Figure 5 **d**, the runtime library translates the pLUTo pseudo-instructions it receives as input to `pluto_op` instructions, which can be parsed by the pLUTo controller that issues the sequence of row sweep DRAM commands required to execute the pLUTo LUT Query. To achieve this, the runtime library holds bookkeeping records for 1) which operands, and 2) which LUTs are mapped in which memory locations. Using this information, this library is able to perform a direct translation to the `{src, dst, lut_subarray, lut_size, lut_bitwidth}` tuple required to construct each atomic `pluto_op` operation.

6.7. The pLUTo Controller

The pLUTo Controller, which is integrated in the DRAM controller, completes the pLUTo system integration stack by 1) enabling the pLUTo LUT Query operation mode for DRAM subarrays prior to the execution of pLUTo LUT Queries (this signals to the subarray that the match logic should be used, and that a row sweep sequence is about to take place), 2) translating `pluto_op` operations to a sequence of DRAM activate and precharge commands, and 3) disabling the pLUTo LUT Query operation mode for DRAM subarrays upon completion of the operation (which ensures that these subarrays can once again be used exclusively for data storage and retrieval).

6.8. Limitations of the pLUTo System Integration Stack

Address Translation. Ensuring the physical proximity of the intervening source, LUT and destination memory addresses associated with a pLUTo LUT Query requires knowledge of their corresponding physical addresses. This challenge can be overcome with the use of our proposed `pluto_alloc` operation, which ensures the correct layout and placement of data in memory. The operating system can be made aware of the physical mapping of the involved memory subarrays, banks and ranks, either 1) by employing the help of a memory controller which is able to provide this information as required, or 2) with an *a priori* reverse-engineering effort that allows the memory mapping scheme to be recovered (e.g., as proposed by [23]). Since the memory allocations are registered in the CPU's TLB (given that the pLUTo instructions are issued to the pLUTo controller by the CPU), the CPU cannot overwrite pLUTo-specific data, since the two co-exist in the same memory address space.

Coherence. pLUTo does not provide a mechanism to enforce coherence between the data stored in pLUTo subarrays and the data stored in other locations in the system (e.g., CPU caches, GPU memory, accelerator memory, secondary storage). For this reason, coherence is managed implicitly, by locking any CPU-side changes to data structures which are currently allocated to pLUTo. This is analogous to prior mechanisms in GPU programming [29, 123].

7. Methodology

We evaluate the three proposed designs of pLUTo (pLUTo-GSA, pLUTo-BSA and pLUTo-GMC). Our implementations assume the parallel operation of 16 subarrays with 8 kB row buffers for DDR4 pLUTo and 512 subarrays with 256 B row buffers for 3D-stacked (HMC-based [100]) pLUTo. Despite the difference in subarray count and row buffer size between the DDR4 and 3DS configurations, they provide the *same effective parallelism at the operation level*, and therefore constitute comparable design points. We compare the performance of each pLUTo configuration against four baselines: 1) a state-of-the-art CPU implementation, 2) a state-of-the-art GPU implementation, 3) an implementation in a near-data processing (NDP) accelerator, 4) an implementation in an FPGA.

7.1. Evaluation Frameworks

We evaluate the CPU and GPU baselines on real systems. We evaluate the FPGA baseline using high-level synthesis (HLS) implementations of the evaluated workloads, created with Vitis 2020.1 [126] and Vivado 2020.1 [127], and perform a post-synthesis simulation for a state-of-the-art Xilinx Zynq UltraScale ZCU102 FPGA [125]. For the evaluation of the NDP baseline, we simulate an HMC-based system [62] with support for bulk bitwise operations as described in [108], and shifting as described in [83]. We simulate various configurations of pLUTo on both DDR4 [65] and HMC [62] memory models using a custom-built simulator, which we plan to release under an open source license. Our simulator estimates the performance of pLUTo operations by parsing the sequence of memory commands required to perform them and enforcing the memory’s timing parameters. The simulator then outputs the total time elapsed to complete the sequence of commands, as well as the energy consumption of the memory during the course of the operation. We evaluate the energy consumption and area overhead of pLUTo configurations using CACTI 7 [22] DDR4 and HMC models. These models supply the energy consumption of each memory command and the area of each memory component. Using these values, we extrapolated pLUTo’s energy consumption and area overhead by considering the transistor count associated with the logic required to implement its functionality, including 1) the addition of the match logic, 2) modifications to the subarray architecture and memory controller, and 3) the addition of the pLUTo controller. Table 2 shows the main parameters that we use in our evaluations.

Table 2: System configuration for simulations.

Parameter	Configuration
Processor	Intel Xeon Gold 5118 [63]
Last-Level Cache	64-Byte cache line, 8-way set-associative, 16.5MB
Main Memory	DDR4 2400MHz, 8GB, 1-channel, 1-rank, 4-bank groups, 4-banks per bank group, 512 rows per subarray, 8 kB per row
Main Memory Timings	17-17-17 (14.16 ns)
GPU	NVIDIA GeForce RTX 2080 Ti [91]
NDP	HMC Model [62], 1.25 GHz on-die core clock, 10 W on-die core TDP, with support for bitwise operations [108] and bit shifting [83].
FPGA	Zynq UltraScale+ MPSoC ZCU102 [125]
pLUTo	16-subarray parallelism unless stated otherwise

7.2. Workloads

Table 3 shows the names and characteristics of the workloads we analyze. Many of these workloads require the execution of operations which cannot be executed trivially using existing Processing-using-Memory designs, and which pLUTo implements using LUT-based computing. Examples of these challenging operations include 1) substitution tables, as required by cipher algorithms such as Salsa20 and VMPC, 2) polynomial division, required by the CRC algorithm, and 3) image binarization, which in prior bulk bitwise accelerator proposals require several bit masking steps and large sequences of bitwise logical operations. All workloads used 100MB of input data except when stated otherwise in the table below. We determined this size to be representative for modern applications while simultaneously highlighting the limitations of the existing memory hierarchy by limiting the cache utilization. For this input size, the relative time spent loading LUTs relative to computation is about 2.5%.

Table 3: Evaluated workloads.

Name	Parameters
Vector Addition, LUT-based [117]	Element width: 4 bits
Vector Point-Wise Multiplication [117]	Q Format: Q1.7, Q1.15
Bitwise Logic (NOT, AND, OR, XOR, XNOR)	# LUT entries: 4
Bit Counting	BC-4: 4 bits, 16-entry LUT; BC-8: 8 bits, 256-entry LUT
CRC-8/16/32 [120]	Packet size: 128 bytes
Salsa20 [24], VMPC [136]	Packet size: 512 bytes
Image Binarization	3-channel 8-bit image, 936000 pixels; threshold: 50%
Color Grading	One 3-channel 8-bit image, 936000 pixels; 8-bit to 8-bit

8. Evaluation

In this section, we evaluate pLUTo’s correct operation (Section 8.1), performance (Section 8.2), energy efficiency (Section 8.3), and area overhead (Section 8.4). We also carry out performance sensitivity analyses to understand the cost of loading LUTs (Section 8.5). Finally, we discuss how pLUTo compares to prior works (Section 8.6).

8.1. SPICE Simulation

We carried out circuit-level SPICE simulations using DRAM cell models to verify the correct functionality of pLUTo. Our results show that the proposed changes *do not introduce* errors in DRAM operation. The observed disturbances to the final voltage in the bitline after the activation of a row correspond to 0.9% of the reference value.

8.2. Performance

Figure 6 plots absolute speedups relative to the CPU, GPU, and NDP baselines for the considered pLUTo design points. We make three key observations. First, we observe that, for the DDR4 (3DS) implementation, the pLUTo-BSA/pLUTo-GMC designs outperform the GPU baseline by $1.53\times$ ($2.12\times$) / $18.38\times$ ($25.52\times$), and the NDP baseline by $3.02\times$ ($4.20\times$) / $36.34\times$ ($50.52\times$), respectively; pLUTo-GSA (both DDR4- and 3DS-based) performs comparably to the GPU and outperforms the NDP baseline. Second, we observe that the 3DS-based pLUTo consistently outperforms its DDR4 counterparts, due to HMC’s lower value of t_{RC} and therefore faster overall lut querying times. Third, we observe that the CRC workloads show the least overall benefit from execution in pLUTo. The speedup in these workloads is bottlenecked by a serial reduction step, which must be performed in the CPU (2D pLUTo) or in the logic layer (pLUTo-3DS). Nevertheless, the acceleration of the parallel portion of the CRC workloads still allows nearly all pLUTo design points to achieve performance comparable to that of the GPU baseline.

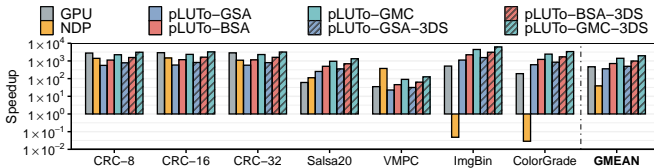


Figure 6: Speedup of GPU, NDP, and pLUTo relative to the baseline CPU. pLUTo parallelizes operations across 16 subarrays. The y-axis uses a logarithmic scale; higher is better.

8.2.1. Performance per Area. Figure 7 shows the speedup per unit area of each pLUTo configuration, relative to the CPU, NDP, and GPU baselines. Area values for the CPU/GPU baselines refer to total chip area for each of these devices, while area values for the NDP baselines refer to the total area available in the logic layer of 3D-stacked memories (4.4 mm^2 per vault in HMC-like devices [26, 27, 62]). We make three key observations. First, all pLUTo designs outperform the GPU and NDP, on average. This improvement is considerably greater than the one observed in Figure 6, when normalized to the area of each design. Second, the performance improvement of pLUTo-3DS is less noticeable in this plot. This leads to the observation that the performance of pLUTo is roughly proportional to the area of the memory technology in which it is implemented, at least for the well-established DDR4 and HMC memory technologies considered in our evaluation. Third, we especially observe improvements for the most memory-

intensive workloads, which for this set are Salsa20 and VMPC. This demonstrates the benefit of performing computation in-memory for workloads that are especially data-intensive.

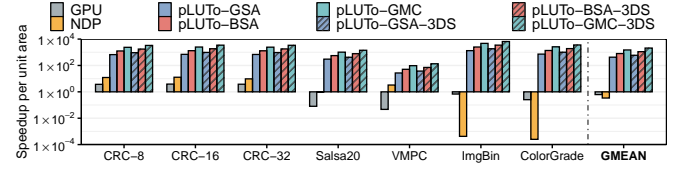


Figure 7: Normalized speedup of GPU, NDP, and pLUTo relative to CPU. pLUTo parallelizes operations across 16 subarrays. The y-axis uses a logarithmic scale; higher is better.

8.2.2. Comparison with FPGA. FPGAs often provide superior performance and energy efficiency. Since they implement logic functionality using LUTs, as pLUTo does, it is important to compare the performance of the two approaches. Figure 8 shows performance of pLUTo compared to the baseline FPGA implementation. We observe that pLUTo is able to outperform the baseline in this scenario for all considered workloads. As expected, the greatest gains are observed for workloads that rely on smaller LUTs (e.g., BC4, ImgBin), and the smallest gains correspond to operations with large input bit widths (e.g., MUL16).

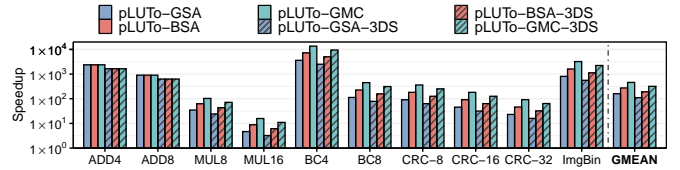


Figure 8: pLUTo speedup relative to FPGA baseline.

8.3. Energy Efficiency

Figure 9 shows the energy efficiency achieved when executing each of the evaluated workloads on different pLUTo configurations. We report the energy consumption for the GPU and NDP baselines, and for all proposed 2D and 3D pLUTo designs. We make two key observations. First, the average energy consumption of the GPU implementation is higher than pLUTo, but lower than pLUTo-3DS. This is because HMC memory is comprised of smaller rows, which increases the overall number of activations required and consequently, the overall energy consumption. Second, we observe that pLUTo is able to outperform the GPU for most simple operations (e.g., ImgBin), but falls short as operation complexity increases (e.g., CRC). This trend is consistent with our observations relative to workload performance discussed earlier in this section.

8.4. Area Overhead

Table 4 shows a breakdown of the estimated area overheads, per DRAM component. These estimates are derived from transistor counts and the area models of CACTI 7 [22].

pLUTo-BSA. We estimate that the sense amplifier switch and FF (shown in Figure 2 (c)) incur a 60% area overhead for the sense amplifiers. The total overhead of pLUTo-BSA is 16.7% of the DRAM chip area.

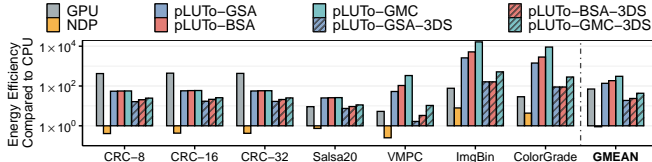


Figure 9: Energy efficiency of GPU, NDP, and pLUTo compared to the baseline CPU. pLUTo parallelizes operations across 16 subarrays. The y-axis uses a logarithmic scale; higher is better.

pLUTo-GMC. The estimated area overhead per 2T1C DRAM cell (shown in Figure 4 (a)) is 25%. The total area overhead of pLUTo-GMC is 23.1% of the DRAM chip area.

pLUTo-GSA. The estimated area overhead of the switch (shown in Figure 4 (b)) is 20% of the area of a sense amplifier, per bitline. The total area overhead of pLUTo-GSA is 10.2% of the DRAM chip area.

Table 4: Area breakdown of a commodity DRAM chip and of the three pLUTo designs (GSA, BSA, GMC).

	DRAM	pLUTo-GSA	pLUTo-BSA	pLUTo-GMC
DRAM Cell	45.23	45.23	45.23	56.53
Local WL Driver	12.45	17.06	17.06	17.06
Sense Amplifier	11.39	13.67	18.23	11.39
Other	1.16	1.49	1.49	1.49
Total	70.23	77.44 (+10.2%)	82.00 (+16.7%)	86.47 (+23.1%)

8.5. LUT Loading Overhead

Figure 10 shows the fraction of total computation time spent loading LUT data (y-axis), relative to the total volume of data that is queried (x-axis). For example, to query around 20 MB worth of data from scratch (x-axis), roughly 10% of the execution time would be spent loading the data into memory (y-axis), and 90% of the execution time would be spent performing pLUTo LUT Queries. We make two key observations. First, we observe that it is sufficient to process 1.9 MB of data (◆ in Figure 10) for the LUT loading time to equal the LUT query time. Second, we observe that, as the volume of data to be processed increases, the fraction of time spent loading the LUTs into memory quickly decreases. For example, for 120 MB (▲ in Figure 10), the fraction of time spent with LUT loading is about 2%.

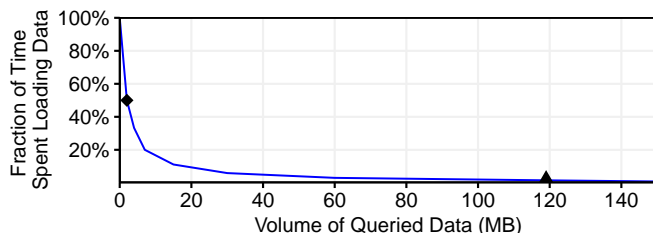


Figure 10: Fraction of time spent setting up LUTs as a function of the volume of data to be queried.

8.6. Comparison With Prior Works

As summarily demonstrated in Table 5 and discussed in Section 3, prior PuM architectures (e.g., [34, 83, 108]) achieve very high throughput and energy efficiency, but do so while supporting a very limited range of operations. These works are

able to address this limitation by exploiting alternatives to conventional bit-parallel algorithms. For example, it is possible to efficiently realize arithmetic operations in Ambit [108] using bit-serial algorithms. Nevertheless, we argue that the additional flexibility afforded by pLUTo’s native support for LUT operations allows it to outperform prior PuM architectures in meaningful and substantive ways. We substantiate this claim with Table 5, which shows the time for each of a set of operations of interest, under each of the architectures mentioned above. In each case, we assume the use of ideal data layouts and report the best-case *achievable* performance for each design. For example, in the case of bitwise operations between input sets A ($a_1 a_2 \dots$) and B ($b_1 b_2 \dots$), under the LUT-based paradigm all input operands are shuffled ($a_1 b_1 a_2 b_2 \dots$), and for all prior PuM designs input sets A and B are ideally stored in two separate memory rows. We note that changes at the system level are required to support the ideal data mapping schemes that maximize pLUTo’s performance. To maximize fairness, the memory capacity for each design is such that the area overheads for all designs remain in a narrow range similar to the overhead of commodity DRAM devices.

Table 5: Comparison of operations supported by pLUTo against prior PuM works. We report values for the pLUTo-BSA implementation, operating in parallel across 4 subarrays. Performance per area and energy efficiency values are normalized to pLUTo-BSA.

	Ambit [108]	SIMDRAM [54]	LAcc [34]	DRISA [83]	pLUTo
Capacity	8 GB	8 GB	8 GB	2 GB	8 GB
Area (mm^2)	61.0	61.1	54.8	65.2	70.5
Power (W)	5.3	5.3	5.3	98.0	11
NOT (<i>ns</i>)	135.0	135.0	135.0	207.6	105.0
AND (<i>ns</i>)	270.0	270.0	270.0	415.2	165.0
OR (<i>ns</i>)	270.0	270.0	270.0	415.2	165.0
XOR (<i>ns</i>)	585.0	585.0	450.0	691.9	165.0
XNOR (<i>ns</i>)	585.0	585.0	450.0	691.9	165.0
Performance Per Area (higher is better)	0.54	0.54	0.67	0.37	1.00
Energy Efficiency (higher is better)	0.54	0.54	0.67	0.02	1.00
4-bit Addition (<i>ns</i>)	5081.0	1585.0	1142.3	1756.5	1920.0
4-bit Multiplication (<i>ns</i>)	19065.0	7451.0	5365.4	8250.1	1920.0
4-bit Bit Counting (<i>ns</i>)	2936.0	1156.0	-	6649.9	120.0
8-bit Bit Counting (<i>ns</i>)	6901.0	2696.0	-	13580.0	1920.0
Performance Per Area (higher is better)	0.34	0.45	1.00*	0.17	1.00
Energy Efficiency (higher is better)	0.69	0.94	2.00*	0.02	1.00
6-bit to 2-bit LUT Query (<i>ns</i>)	-	-	-	-	480.0
8-bit to 8-bit LUT Query (<i>ns</i>)	-	-	-	-	1920.0
Binarization (<i>ns</i>)	-	-	-	-	1920.0
Exponentiation (<i>ns</i>)	-	-	-	-	1920.0

– indicates that the operation is not supported by the proposed mechanism.

* indicates that the result was obtained from partial data.

We draw three key conclusions from Table 5. First, we observe that due to their complexity some operations (e.g., binarization, exponentiation) cannot be implemented in a time-efficient manner using any prior designs. In pLUTo, it is possible to perform exponentiation with high efficiency when operating on small bit widths (for best results, up to 8 bits). Second, we observe that pLUTo performs bitwise logic operations at rates that match or exceed those of all prior works. This result is consequential since it shows that, with proper data alignment, LUT-based computing outperforms even specialized designs. Third, we observe that pLUTo consistently outperforms all three other approaches for most of the con-

sidered operations, in performance (absolute and normalized to area) as well as in energy efficiency. This improvement is not universal: for instance, pLUTo slightly lags behind all baselines in the case of 4-bit addition.

9. Case Study: Binary Neural Networks

As shown in Section 8, pLUTo is especially well-suited for executing limited-precision operations efficiently, since these operations can be expressed using small LUTs. Building on this observation, in this section we validate the applicability of pLUTo for quantized neural networks, an emerging machine learning application. As a proof-of-concept, we evaluate a quantized version of the LeNet-5 network to classify digits from the MNIST dataset. The inference times for CPU, GPU and pLUTo are shown in Table 6. For this evaluation, the CPU is unchanged from Table 2; the GPU is a server-grade NVIDIA P100, commonly used for machine learning applications, with 16GB of dedicated memory. We make two key observations. First, pLUTo-16 outperforms both the CPU (10 \times , 30 \times for 1-bit, 4-bit), the GPU (2 \times , 7 \times) and the FPGA (6 \times , 19 \times) in inference time. This is because pLUTo operations on reduced bit width data are especially efficient, since they can be performed in-place as a short sequence of DRAM commands. Second, pLUTo-16 also achieves considerable energy savings over both the CPU (110 \times , 109 \times), the GPU (80 \times , 81 \times) and the FPGA (15 \times , 16 \times), for both 1- and 4-bit precision. This reduction can be attributed to the overall mitigation in data movement, since most operations are performed in-place. These results strengthen the case for the use of pLUTo in heavily energy-constrained devices, such as IoT and other edge devices.

Table 6: LeNet-5 inference times (in μ s) and energy (in mJ) for CPU, GPU, FPGA and pLUTo.

Bit Width	Accuracy [68]	CPU		GPU		FPGA		pLUTo-BSA-16	
		Time	Energy	Time	Energy	Time	Energy	Time	Energy
1 bit	97.4 %	249	2.2	56	1.6	141	0.3	23	0.02
4 bits	99.1 %	997	8.7	224	6.5	563	1.3	30	0.08

10. Related Work

To our knowledge, pLUTo is the first work to propose a mechanism to enable the efficient bulk querying of LUTs inside DRAM to enable the PuM-based execution of complex operations. In this section, we describe relevant prior works.

Processing-using-Memory (PuM). Many prior works propose various forms of compute-capable memory [1, 2, 4–21, 25, 27, 30, 31, 33, 34, 36, 38–46, 48, 49, 51, 53–61, 67, 70–73, 76–78, 81–84, 86, 90, 94–97, 102–104, 106–112, 115, 118, 124, 128–133, 135]. All these approaches provide significant performance and energy improvements, but focus only on a reduced set of operations, e.g. data movement [30, 107], bulk bitwise operations [1, 84, 108, 128] or neural network acceleration [33, 34, 38, 83]. By combining the in-memory pLUTo LUT Query with the fast and efficient bitwise logic and shifting operations enabled by these prior works, pLUTo provides support for a much greater range of

operations. While pPIM [114] and LAcc [34], for example, leverage dedicated LUT hardware for neural network acceleration, the pLUTo LUT Query is suitable for a greater range of operations (by supporting wider input-output configurations, with greater throughput and efficiency.) In contrast to pPIM and LAcc, DRAF [47] employs a DRAM-based FPGA-like LUT-based computing paradigm. DRAF outperforms FPGA execution in area and energy efficiency, but lags behind in throughput and latency. In contrast, pLUTo enables high-throughput LUT queries, without compromising energy efficiency. Furthermore, pLUTo subarrays can operate as a conventional storage medium when not partaking in a pLUTo LUT Query, so there is no compromise in DRAM capacity, aside from the area increase for the modifications required by pLUTo.

Processing-near-Memory (PnM). 3D-stacked memories [2, 28, 69, 98, 134] are an emerging technology that enables the vertical stacking of memory layers coupled to a logic layer. This technology provides higher bandwidth compared to 2D DRAM. pLUTo is a *complementary* technology to 3D-stacked memory: indeed, the two can be combined, as shown in Section 8.

11. Conclusion

We introduced pLUTo, a DRAM-based PuM architecture that enables the energy-efficient storage and bulk query of lookup tables. We build pLUTo based on the key observation that enabling in-DRAM LUT-based provides a flexible substrate to efficiently execute complex operations within DRAM. We provide (i) the hardware design of three different pLUTo architectures, each one targeting different performance metrics (i.e., throughput, energy, and area); and (ii) the required system integration support to enable the execution of in-DRAM pLUTo operations. We evaluate pLUTo against four different baseline systems using a broad range of applications. Our evaluation shows that pLUTo outperforms the baseline CPU-, GPU-, FPGA-, PnM- and PuM-based systems. We believe that the adoption of pLUTo in real systems will provide significant performance and energy improvements in applications designed to take advantage of it.

Acknowledgments

We thank the anonymous reviewers of HPCA 2019, ICCD 2020, HPCA 2020, ISCA 2020, ISCA 2021, MICRO 2021, and ASPLOS 2022 for their valuable comments and feedback. We thank the SAFARI Research Group members for valuable feedback and the stimulating intellectual environment they provide. We acknowledge the generous gifts provided by our industrial partners: Google, Huawei, Intel, Microsoft, and VMware.

This work was funded in part by the Instituto de Telecomunicações and the Fundação para a Ciência e a Tecnologia (FCT), under grant number UIDB/50008/2020-UIDP/50008/2020.

References

- [1] S. Aga, S. Jeloka, A. Subramaniyan, S. Narayanasamy, D. Blaauw, and R. Das, "Compute Caches," in *HPCA*, 2017.
- [2] J. Ahn, S. Hong, S. Yoo, O. Mutlu, and K. Choi, "A Scalable Processing-In-Memory Accelerator For Parallel Graph Processing," in *ISCA*, 2015.
- [3] A. V. Aho, R. Sethi, and J. D. Ullman, *Compilers, Principles, Techniques*. Addison Wesley, 1986.
- [4] A. Akerib, A. Oren, E. Ehrman, and M. Meyassed, "Using Storage Cells To Perform Computation," 2012, US Patent 8,238,173.
- [5] S. Angizi, N. A. Fahmi, W. Zhang, and D. Fan, "PIM-Assembler: A Processing-In-Memory Platform For Genome Assembly," in *DAC*, 2020.
- [6] S. Angizi and D. Fan, "IMC: Energy-Efficient In-Memory Convolver For Accelerating Binarized Deep Neural Network," in *NCS*, 2017.
- [7] —, "Deep Neural Network Acceleration In Non-Volatile Memory: A Digital Approach," in *NANOARCH*, 2019.
- [8] —, "GraphiDe: A Graph Processing Accelerator Leveraging In-DRAM Computing," in *GLSVLSI*, 2019.
- [9] —, "ReDRAM: A Reconfigurable Processing-In-DRAM Platform For Accelerating Bulk Bit-Wise Operations," in *ICCAD*, 2019.
- [10] S. Angizi, Z. He, N. Bagherzadeh, and D. Fan, "Design And Evaluation Of A Spintronic In-Memory Processing Platform For Nonvolatile Data Encryption," in *IEEE TCAD*, 2017.
- [11] S. Angizi, Z. He, and D. Fan, "Energy Efficient In-Memory Computing Platform Based On 4-Terminal Spin Hall Effect-Driven Domain Wall Motion Devices," in *GLSVLSI*, 2017.
- [12] —, "DIMA: A Depthwise CNN In-Memory Accelerator," in *ICCAD*, 2018.
- [13] —, "PIMA-Logic: A Novel Processing-In-Memory Architecture For Highly Flexible And Energy-Efficient Logic Computation," in *DAC*, 2018.
- [14] —, "ParaPIM: A Parallel Processing-In-Memory Accelerator For Binary-Weight Deep Neural Networks," in *ASP-DAC*, 2019.
- [15] S. Angizi, Z. He, F. Parveen, and D. Fan, "Rimpa: A New Reconfigurable Dual-Mode In-Memory Processing Architecture With Spin Hall Effect-Driven Domain Wall Motion Device," in *ISVLSI*, 2017.
- [16] —, "IMCE: Energy-Efficient Bit-Wise In-Memory Convolution Engine For Deep Neural Network," in *ASP-DAC*, 2018.
- [17] S. Angizi, Z. He, A. S. Rakin, and D. Fan, "CMP-PIM: An Energy-Efficient Comparator-Based Processing-In-Memory Neural Network Accelerator," in *DAC*, 2018.
- [18] S. Angizi, J. Sun, W. Zhang, and D. Fan, "Aligns: A Processing-In-Memory Accelerator For DNA Short Read Alignment Leveraging SOT-MRAM," in *DAC*, 2019.
- [19] —, "GraphS: A Graph Processing Accelerator Leveraging SOT-MRAM," in *DATE*, 2019.
- [20] —, "PIM-Aligner: A Processing-In-Mram Platform For Biological Sequence Alignment," in *DATE*, 2020.
- [21] S. Angizi, W. Zhang, and D. Fan, "Exploring DNA Alignment-In-Memory Leveraging Emerging SOT-MRAM," in *GLSVLSI*, 2020.
- [22] R. Balasubramonian, A. B. Kahng, N. Muralimanohar, A. Shafiee, and V. Srinivas, "Cacti 7: New Tools For Interconnect Exploration In Innovative Off-Chip Memories," in *TACO*, 2017.
- [23] A. Barengi, L. Breveglieri, N. Izzo, and G. Pelosi, "Software-Only Reverse Engineering Of Physical DRAM Mappings For Rowhammer Attacks," in *IVSW*. IEEE, 2018.
- [24] D. J. Bernstein, "Salsa20 Specification," <http://www.ecrypt.eu.org/stream/salsa20pf.html>, 2005.
- [25] D. Bhattacharjee, R. Devadoss, and A. Chattopadhyay, "Revamp: Reram Based Vliw Architecture For In-Memory Computing," in *DATE*, 2017.
- [26] A. Boroumand, S. Ghose, Y. Kim, R. Ausavarungnirun, E. Shiu, R. Thakur, D. Kim, A. Kuusela, A. Knies, P. Ranganathan, and O. Mutlu, "Google Workloads For Consumer Devices: Mitigating Data Movement Bottlenecks," in *ASPLOS*, 2018.
- [27] A. Boroumand, S. Ghose, M. Patel, H. Hassan, B. Lucia, R. Ausavarungnirun, K. Hsieh, N. Hajinazar, K. T. Malladi, H. Zheng *et al.*, "Conda: Efficient Cache Coherence Support For Near-Data Accelerators," in *ISCA*, 2019.
- [28] A. Boroumand, S. Ghose, M. Patel, H. Hassan, B. Lucia, K. Hsieh, K. T. Malladi, H. Zheng, and O. Mutlu, "LazyPIM: An Efficient Cache Coherence Mechanism For Processing-In-Memory," in *CAL*, 2016.
- [29] A. R. Brodtkorb, T. R. Hagen, and M. L. Sætra, "Graphics Processing Unit (GPU) Programming Strategies And Trends In GPU Computing," *Journal of Parallel and Distributed Computing*, vol. 73, no. 1, pp. 4–13, 2013.
- [30] K. K. Chang, P. J. Nair, D. Lee, S. Ghose, M. K. Qureshi, and O. Mutlu, "Low-Cost Inter-Linked Subarrays (LISA): Enabling Fast Inter-Subarray Data Movement In DRAM," in *HPCA*, 2016.
- [31] P. Chi, S. Li, C. Xu, T. Zhang, J. Zhao, Y. Liu, Y. Wang, and Y. Xie, "Prime: A Novel Processing-In-Memory Architecture For Neural Network Computation In Reram-Based Main Memory," in *ISCA*, 2016.
- [32] B. Dally, "The Path To Exascale Computing," <http://images.nvidia.com/events/sc15/pdfs/SC5102-path-exascale-computing.pdf>, 2015.
- [33] Q. Deng, L. Jiang, Y. Zhang, M. Zhang, and J. Yang, "DrAcc: A DRAM Based Accelerator For Accurate CNN Inference," in *DAC*, 2018.
- [34] Q. Deng, Y. Zhang, M. Zhang, and J. Yang, "LAcc: Exploiting Lookup Table-Based Fast And Accurate Vector Multiplication In DRAM-Based CNN Accelerator," in *DAC*, 2019.
- [35] F. Devaux, "The True Processing In Memory Accelerator," in *HC*, 2019.
- [36] J. Draper, J. Chame, M. Hall, C. Steele, T. Barrett, J. LaCoss, J. Granacki, J. Shin, C. Chen, C. W. Kang *et al.*, "The Architecture Of The Diva Processing-In-Memory Chip," in *ICS*, 2002.
- [37] M. Drummond, A. Daglis, N. Mirzadeh, D. Ustiugov, J. Picorel, B. Falsafi, B. Grot, and D. Pnevmatikatos, "The Mondrian Data Engine," in *ISCA*, 2017.
- [38] C. Eckert, X. Wang, J. Wang, A. Subramaniyan, R. Iyer, D. Sylvester, D. Blaauw, and R. Das, "Neural Cache: Bit-Serial In-Cache Acceleration Of Deep Neural Networks," in *ISCA*, 2018.
- [39] D. Fan, "Low Power In-Memory Computing Platform With Four Terminal Magnetic Domain Wall Motion Devices," in *NANOARCH*, 2016.
- [40] D. Fan and S. Angizi, "Energy Efficient In-Memory Binary Deep Neural Network Accelerator With Dual-Mode SOT-MRAM," in *ICCD*, 2017.
- [41] D. Fan, S. Angizi, and Z. He, "In-Memory Computing With Spintronic Devices," in *ISVLSI*, 2017.
- [42] D. Fan, Z. He, and S. Angizi, "Leveraging Spintronic Devices For Ultra-Low Power In-Memory Computing: Logic And Neural Network," in *MWSCAS*, 2017.
- [43] D. Fujiki, S. Mahlke, and R. Das, "Duality Cache For Data Parallel Acceleration," in *ISCA*, 2019.
- [44] P.-E. Gaillardon, L. Amarú, A. Siemon, E. Linn, R. Waser, A. Chattopadhyay, and G. De Micheli, "The Programmable Logic-In-Memory (Plim) Computer," in *DATE*, 2016.
- [45] D. Gao, T. Shen, and C. Zhuo, "A Design Framework For Processing-In-Memory Accelerator," in *SLIP*, 2018.
- [46] F. Gao, G. Tziantzioulis, and D. Wentzlauff, "ComputeDRAM: In-Memory Compute Using Off-The-Shelf DRAMs," in *MICRO*, 2019.
- [47] M. Gao, C. Delimitrou, D. Niu, K. T. Malladi, H. Zheng, B. Brennan, and C. Kozyrakis, "Draf: A Low-Power DRAM-Based Reconfigurable Acceleration Fabric," in *ISCA*, 2016.
- [48] S. Ghose, A. Boroumand, J. S. Kim, J. Gómez-Luna, and O. Mutlu, "Processing-In-Memory: A Workload-Driven Perspective," in *IBM J. Res. Dev.*, 2019.
- [49] S. Ghose, K. Hsieh, A. Boroumand, R. Ausavarungnirun, and O. Mutlu, "Enabling The Adoption Of Processing-In-Memory: Challenges, Mechanisms, Future Research Directions," in *Beyond-CMOS Technologies for Next Generation Computer Design*, 2018.
- [50] —, "The Processing-In-Memory Paradigm: Mechanisms To Enable Adoption," in *Beyond-CMOS Technologies for Next Generation Computer Design*, 2019.
- [51] M. Gokhale, B. Holmes, and K. Jobst, "Processing In Memory: The Terasys Massively Parallel PIM Array," in *Computer*, 1995.
- [52] J. Gómez-Luna, I. E. Hajj, I. Fernandez, C. Giannoula, G. F. Oliveira, and O. Mutlu, "Benchmarking a New Paradigm: An Experimental Analysis of a Real Processing-in-Memory Architecture," *arXiv preprint arXiv:2105.03814*, 2021.
- [53] P. Gu, X. Xie, S. Li, D. Niu, H. Zheng, K. T. Malladi, and Y. Xie, "DLUX: A LUT-Based Near-Bank Accelerator For Data Center Deep Learning Training Workloads," in *TCAD*, 2020.
- [54] N. Hajinazar, G. F. Oliveira, S. Gregorio, J. D. Ferreira, N. M. Ghiasi, M. Patel, M. Alser, S. Ghose, J. Gómez-Luna, and O. Mutlu, "SIMDRAM: A Framework For Bit-Serial Simd Processing Using DRAM," in *HPCA*, 2021.
- [55] S. Hamdioui, S. Kvatinisky, G. Cauwenberghs, L. Xie, N. Wald, S. Joshi, H. M. Elsayed, H. Corporaal, and K. Bertels, "Memristor For Computing: Myth Or Reality?" in *DATE*, 2017.
- [56] S. Hamdioui, L. Xie, H. A. Du Nguyen, M. Taouil, K. Bertels, H. Corporaal, H. Jiao, F. Catthoor, D. Wouters, L. Eike *et al.*, "Memristor Based Computation-In-Memory Architecture For Data-Intensive Applications," in *DATE*, 2015.
- [57] Z. He, S. Angizi, and D. Fan, "Exploring Stt-Mram Based In-Memory Computing Paradigm With Application Of Image Edge Extraction," in *ICCD*, 2017.
- [58] Z. He, S. Angizi, F. Parveen, and D. Fan, "High Performance And Energy-Efficient In-Memory Computing Architecture Based On SOT-MRAM," in *NANOARCH*, 2017.
- [59] —, "Leveraging Dual-Mode Magnetic Crossbar For Ultra-Low Energy In-Memory Data Encryption," in *GLSVLSI*, 2017.

- [60] K. Hsieh, E. Ebrahimi, G. Kim, N. Chatterjee, M. O'Connor, N. Vijaykumar, O. Mutlu, and S. W. Keckler, "Transparent Offloading And Mapping (Tom) Enabling Programmer-Transparent Near-Data Processing In GPU Systems," in *ISCA*, 2016.
- [61] K. Hsieh, S. Khan, N. Vijaykumar, K. K. Chang, A. Boroumand, S. Ghose, and O. Mutlu, "Accelerating Pointer Chasing In 3D-Stacked Memory: Challenges, Mechanisms, Evaluation," in *ICCD*, 2016.
- [62] Hybrid Memory Cube Consortium, "Hybrid Memory Cube Specification 2.1," Tech. Rep., 2014.
- [63] Intel, "Intel® Xeon® Gold 5118 Processor Specifications." [Online]. Available: <https://www.intel.com/content/www/us/en/products/sku/120473/intel-xeon-gold-5118-processor-16-5m-cache-2-30-ghz/specifications.html>
- [64] JEDEC, "DDR3 SDRAM Standard, JESD79-3d," <https://www.jedec.org/standards-documents/docs/jesd-79-3d>, 2012.
- [65] —, "DDR4 SDRAM Standard, JESD79-4b," <https://www.jedec.org/standards-documents/docs/jesd79-4a>, 2017.
- [66] S. Kanev, J. P. Darago, K. Hazelwood, P. Ranganathan, T. Moseley, G.-Y. Wei, and D. Brooks, "Profiling A Warehouse-Scale Computer," in *ISCA*, 2015.
- [67] M. Kang, M.-S. Keel, N. R. Shanbhag, S. Eilert, and K. Curewitz, "An Energy-Efficient VLSI Architecture For Pattern Recognition Via Deep Embedding Of Computation In Sram," in *ICASSP*, 2014.
- [68] S. Khoram and J. Li, "Adaptive Quantization Of Neural Networks," in *ICLR*, 2018.
- [69] D. Kim, J. Kung, S. Chai, S. Yalamanchili, and S. Mukhopadhyay, "Neurocube: A Programmable Digital Neuromorphic Architecture With High-Density 3D Memory," in *ISCA*, 2016.
- [70] Y. Kim, V. Seshadri, D. Lee, J. Liu, and O. Mutlu, "A Case For Exploiting Subarray-Level Parallelism (SALP) In DRAM," in *ISCA*, 2012.
- [71] S. Kvatinsky, D. Belousov, S. Liman, G. Satat, N. Wald, E. G. Friedman, A. Kolodny, and U. C. Weiser, "Magic—Memristor-Aided Logic," in *TCAS II*, 2014.
- [72] S. Kvatinsky, A. Kolodny, U. C. Weiser, and E. G. Friedman, "Memristor-Based Imply Logic Design Procedure," in *ICCD*, 2011.
- [73] S. Kvatinsky, G. Satat, N. Wald, E. G. Friedman, A. Kolodny, and U. C. Weiser, "Memristor-Based Material Implication (Imply) Logic: Design Principles And Methodologies," in *VLSI*, 2013.
- [74] Y.-C. Kwon, S. H. Lee, J. Lee, S.-H. Kwon, J. M. Ryu, J.-P. Son, O. Seongil, H.-S. Yu, H. Lee, S. Y. Kim *et al.*, "A 20nm 6gb Function-In-Memory DRAM, Based On Hbm2 With A 1.2 Tflops Programmable Computing Unit Using Bank-Level Parallelism, For Machine Learning Applications," in *ISSCC*, 2021.
- [75] P. S. Lazar and S. C. Oh, "DRAM With Total Self Refresh And Control Circuit," 2004, US Patent 6,741,515.
- [76] P. V. Lea, "Apparatuses And Methods For In-Memory Operations," 2019, US Patent 10,268,389.
- [77] B. C. Lee, E. Ipek, O. Mutlu, and D. Burger, "Phase Change Memory Architecture And The Quest For Scalability," in *CACM*, 2010.
- [78] B. C. Lee, P. Zhou, J. Yang, Y. Zhang, B. Zhao, E. Ipek, O. Mutlu, and D. Burger, "Phase-Change Technology And The Future Of Main Memory," in *MICRO*, 2010.
- [79] D. U. Lee, K. W. Kim, K. W. Kim, H. Kim, J. Y. Kim, Y. J. Park, J. H. Kim, D. S. Kim, H. B. Park, J. W. Shin *et al.*, "A 1.2v 8gb 8-Channel 128 Gb/S High-Bandwidth Memory (Hbm) Stacked DRAM With Effective Microbump I/O Test Methods Using 29nm Process And Tsv," in *ISSCC*, 2014.
- [80] C. Lefurgy, K. Rajamani, F. Rawson, W. Felter, M. Kistler, and T. W. Keller, "Energy Management For Commercial Servers," in *Computer*, 2003.
- [81] Y. Levy, J. Bruck, Y. Cassuto, E. G. Friedman, A. Kolodny, E. Yaakobi, and S. Kvatinsky, "Logic Operations In Memory Using A Memristive Akers Array," in *Microelectronics Journal*, 2014.
- [82] S. Li, A. O. Glova, X. Hu, P. Gu, D. Niu, K. T. Malladi, H. Zheng, B. Brennan, and Y. Xie, "Scope: A Stochastic Computing Engine For DRAM-Based In-Situ Accelerator," in *MICRO*, 2018.
- [83] S. Li, D. Niu, K. T. Malladi, H. Zheng, B. Brennan, and Y. Xie, "Drisa: A DRAM-Based Reconfigurable In-Situ Accelerator," in *MICRO*, 2017.
- [84] S. Li, C. Xu, Q. Zou, J. Zhao, Y. Lu, and Y. Xie, "Pinatubo: A Processing-In-Memory Architecture For Bulk Bitwise Operations In Emerging Non-Volatile Memories," in *DAC*, 2016.
- [85] G. H. Loh, "3D-Stacked Memory Architectures For Multi-Core Processors," in *ISCA*, 2008.
- [86] T. A. Manning, "Apparatuses And Methods For Comparing Data Patterns In Memory," 2018, US Patent 9,934,856.
- [87] Micron, "Micron Collaborates With Broadcom To Solve DRAM Timing Challenge, Delivering Improved Performance For Net-
- working Customers," <http://investors.micron.com/static-files/3e9669f9-7186-481c-8594-dca7e992a0b2>, 2013.
- [88] O. Mutlu, S. Ghose, J. Gómez-Luna, and R. Ausavarungnirun, "Enabling Practical Processing In And Near Memory For Data-Intensive Computing," in *DAC*, 2019.
- [89] —, "Processing Data Where It Makes Sense: Enabling In-Memory Computation," in *Microprocessors and Microsystems*, 2019.
- [90] O. Mutlu, S. Ghose, J. Gómez-Luna, and R. Ausavarungnirun, "A Modern Primer On Processing In Memory," in *Emerging Computing: From Devices To Systems - Looking Beyond Moore and Von Neumann*, 2021.
- [91] Nvidia, "Nvidia GeForce RTX 2080 Ti Graphics Card." [Online]. Available: <https://www.nvidia.com/en-eu/geforce/graphics-cards/rtx-2080-ti/>
- [92] G. F. Oliveira, J. Gómez-Luna, L. Orosa, S. Ghose, N. Vijaykumar, I. Fernandez, M. Sadrosadati, and O. Mutlu, "DAMOV: A New Methodology And Benchmark Suite For Evaluating Data Movement Bottlenecks," *arXiv:2105.03725 [cs.AR]*, 2021.
- [93] D. Pandiyan and C. Wu, "Quantifying The Energy Cost Of Data Movement For Emerging Smart Phone Workloads On Mobile Platforms," in *ISWC*, Oct. 2014.
- [94] F. Parveen, S. Angizi, Z. He, and D. Fan, "Low Power In-Memory Computing Based On Dual-Mode SOT-MRAM," in *ISLPEd*, 2017.
- [95] —, "Imcs2: Novel Device-To-Architecture Co-Design For Low-Power In-Memory Computing Platform Using Coterminous Spin Switch," in *IEEE Trans. Magn.*, 2018.
- [96] F. Parveen, Z. He, S. Angizi, and D. Fan, "Hybrid Polymorphic Logic Gate With 5-Terminal Magnetic Domain Wall Motion Device," in *ISVLSI*, 2017.
- [97] —, "Hieim: Highly Flexible In-Memory Computing Using Stt Mram," in *ASP-DAC*, 2018.
- [98] A. Pattnaik, X. Tang, A. Jog, O. Kayiran, A. K. Mishra, M. T. Kandemir, O. Mutlu, and C. R. Das, "Scheduling Techniques For GPU Architectures With Processing-In-Memory Capabilities," in *PACT*, 2016.
- [99] I. Paul, W. Huang, M. Arora, and S. Yalamanchili, "Harmonia: Balancing Compute And Memory Power In High-Performance GPUs," in *ISCA*, 2015.
- [100] J. T. Pawlowski, "Hybrid Memory Cube (Hmc)," in *HCS*, 2011.
- [101] Y. Peng, B. W. Ku, Y. Park, K.-I. Park, S.-J. Jang, J. S. Choi, and S. K. Lim, "Design, Packaging, and Architectural Policy Co-optimization for DC Power Integrity in 3D DRAM," in *DAC*, 2015.
- [102] A. S. Rakin, S. Angizi, Z. He, and D. Fan, "PIM-TGAN: A Processing-In-Memory Accelerator For Ternary Generative Adversarial Networks," in *ICCD*, 2018.
- [103] A. K. Ramanathan, G. S. Kalsi, S. Srinivasa, T. M. Chandran, K. R. Pillai, O. J. Omer, V. Narayanan, and S. Subramoney, "Look-Up Table Based Energy Efficient Processing In Cache Support For Neural Network Acceleration," in *MICRO*, 2020.
- [104] S. H. S. Rezaei, M. Modarressi, R. Ausavarungnirun, M. Sadrosadati, O. Mutlu, and M. Daneshzad, "NoM: Network-On-Memory For Inter-Bank Data Transfer In Highly-Banked Memories," in *CAL*, 2020.
- [105] P. Rosenfeld, "Performance Exploration Of The Hybrid Memory Cube," Ph.D. dissertation, 2014.
- [106] V. Seshadri, K. Hsieh, A. Boroumand, D. Lee, M. A. Kozuch†, O. Mutlu, P. B. Gibbons, and T. C. Mowry, "Fast Bulk Bitwise And And Or In DRAM," in *CAL*, 2015.
- [107] V. Seshadri, Y. Kim, C. Fallin, D. Lee, R. Ausavarungnirun, G. Pekhimenko, Y. Luo, O. Mutlu, P. B. Gibbons, M. A. Kozuch, and Others, "RowClone: Fast And Energy-Efficient In-DRAM Bulk Data Copy And Initialization," in *MICRO*, 2013.
- [108] V. Seshadri, D. Lee, T. Mullins, H. Hassan, A. Boroumand, J. Kim, M. A. Kozuch, O. Mutlu, P. B. Gibbons, and T. C. Mowry, "Ambit: In-Memory Accelerator For Bulk Bitwise Operations Using Commodity DRAM Technology," in *MICRO*, 2017.
- [109] V. Seshadri, T. Mullins, A. Boroumand, O. Mutlu, P. B. Gibbons, M. A. Kozuch, and T. C. Mowry, "Gather-Scatter DRAM: In-DRAM Address Translation To Improve The Spatial Locality Of Non-Unit Strided Accesses," in *MICRO*, 2015.
- [110] V. Seshadri and O. Mutlu, "Simple Operations In Memory To Reduce Data Movement," in *Adv. Comput.*, 2017.
- [111] —, "In-DRAM Bulk Bitwise Execution Engine," in *arXiv preprint arXiv:1905.09822*, 2019.
- [112] A. Shafiee, A. Nag, N. Muralimanohar, R. Balasubramonian, J. P. Strachan, M. Hu, R. S. Williams, and V. Srikumar, "Isaac: A Convolutional Neural Network Accelerator With In-Situ Analog Arithmetic In Crossbars," in *ISCA*, 2016.
- [113] P. Siegl, R. Buchty, and M. Berekovic, "Data-Centric Computing Frontiers: A Survey On Processing-In-Memory," in *MEMSYS*, 2016.
- [114] P. R. Sutradhar, M. Connolly, S. Bavikadi, S. M. P. Dinakararao, M. A. In-

- dovina, and A. Ganguly, "Ppim: A Programmable Processor-In-Memory Architecture With Precision-Scaling For Deep Learning," in *CAL*, 2020.
- [115] Y. Tian, T. Wang, Q. Zhang, and Q. Xu, "ApproxLUT: A Novel Approximate Lookup Table-Based Accelerator," in *ICCAD*, 2017.
- [116] T. Vogelsang, "Understanding The Energy Consumption Of Dynamic Random Access Memories," in *MICRO*, 2010.
- [117] Q. Wang, X. Zhang, Y. Zhang, and Q. Yi, "Augem: Automatically Generate High Performance Dense Linear Algebra Kernels On X86 CPUs," in *SC*, 2013.
- [118] Y. Wang, L. Orosa, X. Peng, Y. Guo, S. Ghose, M. Patel, J. S. Kim, J. G. Luna, M. Sadrosadati, N. M. Ghiasi *et al.*, "Figaro: Improving System Performance Via Fine-Grained In-DRAM Data Relocation And Caching," in *MICRO*, 2020.
- [119] M. Ware, K. Rajamani, M. Floyd, B. Brock, J. C. Rubio, F. Rawson, and J. B. Carter, "Architecting For Power Management: The IBM®Power7™Approach," in *HPCA*, 2010.
- [120] H. S. Warren, *Hacker's Delight*, 2013.
- [121] D. Weber, A. Thies, U. Kahler, M. Lepper, and R. Schutz, "Current and Future Challenges of DRAM Metallization," in *IITC*, 2005.
- [122] W. A. Wulf and S. A. McKee, "Hitting The Memory Wall: Implications Of The Obvious," in *ACM SIGARCH Computer Architecture News*, 1995.
- [123] S. Xiao and W.-c. Feng, "Inter-Block GPU Communication Via Fast Barrier Synchronization," in *IPDPS*. IEEE, 2010.
- [124] L. Xie, H. A. Du Nguyen, M. Taouil, S. Hamdioui, and K. Bertels, "Fast Boolean Logic Mapped On Memristor Crossbar," in *ICCD*, 2015.
- [125] I. Xilinx, "Zcu102 Evaluation Board: User Guide," https://www.xilinx.com/support/documentation/boards_and_kits/zcu102/ug1182-zcu102-eval-bd.pdf, 2019.
- [126] —, "Vitis 2020.1," <https://www.xilinx.com/products/design-tools/vitis.html>, 2020.
- [127] —, "Vivado 2020.1," <https://www.xilinx.com/products/design-tools/vivado.html>, 2020.
- [128] X. Xin, Y. Zhang, and J. Yang, "ROC: DRAM-Based Processing With Reduced Operation Cycles," in *DAC*, 2019.
- [129] —, "ELP2IM: Efficient And Low Power Bitwise Operation Processing In DRAM," in *HPCA*, 2020.
- [130] L. Yang, S. Angizi, and D. Fan, "A Flexible Processing-In-Memory Accelerator For Dynamic Channel-Adaptive Deep Neural Networks," in *ASP-DAC*, 2020.
- [131] J. Yu, H. A. Du Nguyen, L. Xie, M. Taouil, and S. Hamdioui, "Memristive Devices For Computation-In-Memory," in *DATE*, 2018.
- [132] J. T. Zawodny and G. E. Hush, "Apparatuses And Methods To Reverse Data Stored In Memory," 2018, US Patent 9,959,923.
- [133] Y. Zha and J. Li, "Hyper-Ap: Enhancing Associative Processing Through A Full-Stack Optimization," in *ISCA*, 2020.
- [134] D. Zhang, N. Jayasena, A. Lyashevsky, J. L. Greathouse, L. Xu, and M. Ignatowski, "Top-PIM: Throughput-Oriented Programmable Processing In Memory," in *HPDC*, 2014.
- [135] H. Zhao, A. Goda, K. K. Parat, A. G. Mauri, H. Liu, T. Tanzawa, S. Yamada, and K. Sakui, "Apparatuses And Methods To Control Body Potential In Memory Operations," 2017, US Patent 9,536,618.
- [136] B. Zoltak, "VMPC One-Way Function And Stream Cipher," in *FSE*, 2004.